Characterization of microporous–mesoporous MCM-41 silicates prepared in the presence of octyltrimethylammonium bromide

Abdelhamid Sayari*

Department of Chemical Engineering and CERPIC, Université Laval, Ste-Foy, Qc, Canada G1K 7P4
E-mail: sayari@gch.ulaval.ca

Michal Kruk and Mietek Jaroniec

Department of Chemistry, Kent State University, OH 44242, USA

Received 19 July 1997; accepted 23 October 1997

MCM-41 silicates prepared in the presence of octyltrimethylammonium bromide either by a conventional method or by post-synthesis hydrothermal treatment were characterized by nitrogen adsorption in a wide range of relative pressure from 10^{-6} to 1. Hydrothermally restructured samples were found to have lower BET surface areas, lower external surface areas and thicker silica walls than the non-treated sample. More importantly, in addition to their characteristic mesopores (ca. 3 nm), they were shown to have considerable amounts of micropores. The relative amount of micropores and mesopores was shown to be dependent on the treatment conditions. Thus, it is demonstrated that the postsynthesis hydrothermal restructuring is a convenient synthesis route to MCM-41 silicates with bimodal pore size distribution involving controllable amounts of microporosity.

Keywords: MCM-41, M41S, mesoporous materials, bimodal pore size distribution, thermal restructuring

1. Introduction

Since the discovery of M41S [1,2] and FSM-16 [3] periodic mesoporous silicates, this field underwent explosive growth. Innovative developments have been achieved in many areas including (i) new or improved synthesis strategies for pure and modified silicates [4], (ii) synthesis of non-silica mesostructured materials, specially transition metal oxides [5], (iv) synthesis of mesostructured materials with various forms, such as films [6], fibers [7], spheres [8] and others [9–11], and (v) development of potential applications, particularly in catalysis [12].

Most of the works reported to date used surfactants with alkyl chains having 12 to 18 carbon atoms which yield materials with pore sizes roughly in the range 2.5 to 4 nm. Actually, there is a relatively large gap between the largest pore entrance size of microporous zeolites, i.e., 0.75×1.0 nm for the 14-membered ring of UTD-1 [13] and the smallest channel diameter of MCM-41 silicates which are prepared in the presence of surfactants with 8 or 10 carbon atom chains. Periodic or crystalline silicates with pore sizes between 1 and 2 nm, which are not yet readily accessible through direct synthesis, are likely to be very important for gas separation and shape selective catalysis. Notice that at the lowest end of achievable pore sizes in MCM-41 silicates, the reported values depend strongly on the evaluation method used. Based on the Horváth and Kawazoe model [14], MCM-41 prepared in the presence of octyltrimethylammonium bromide (OTAB) was first reported to have 1.8 nm pores [2]. In our recent study [15], we found that depending on the method used, the calculated pore size of such materials varied from 1.32 nm based on the Barrett–Joyner–Halenda (BJH) method [16] to 2.4 nm based on recently reported data [17] obtained from nonlocal density functional theory (NL DFT). We favored 2.07 nm obtained on the basis of geometrical considerations [15]. More recently, Ravikovitch et al. [18] reported almost identical values for a similar MCM-41 material calculated using the BJH method (1.45 nm) and the pore size calculation method based on theoretical adsorption isotherms obtained from NL DFT (2.4–2.5 nm). Furthermore, both studies [15,18] showed that as the number of carbon atoms in the surfactant alkyl chain decreases, particularly below 12, the intensity and sharpness of the XRD peaks deteriorate significantly indicating the occurrence of excessive broadening of the pore size distribution (PSD).

Our recent study [19] on pore size expansion of MCM-41 materials via the post-synthesis hydrothermal restructuring method reported by Khushalani et al. [20] showed that pore size enlargement was accompanied by a decrease in the primary mesopore surface area, an increase in the primary mesopore volume, pore wall thickening and a significant improvement of pore size uniformity. However, excessive hydrothermal treatment led to the degradation of the porous structure of MCM-41 materials and the development of microporosity. It was also demonstrated that in the early stages of the process, i.e., before the pores actually widen, the external

* To whom correspondence should be addressed.

surface area of the samples decreases markedly. Since the hydrothermal restructuring technique described earlier [19,20] was applied only to MCM-41 silicates prepared in the presence of cetyltrimethylammonium bromide (CTAB), it was interesting to extend it to MCM-41 materials with pore sizes at the lowest end. This paper deals mainly with the characterization of the pore structure of MCM-41 silicates prepared in the presence of OTAB either by a standard method [21] or by post-synthesis hydrothermal treatment [19]. The current study showed that the latter treatment leads to the development of microporosity in addition to the mesopores characteristic of MCM-41 materials. Although, as inferred from X-ray diffraction (XRD) data, the resulting materials did not exhibit a high degree of structural ordering, the occurrence of porous systems with bimodal pore size distributions may be important [22]. In addition, our enhanced ability to control the amount of micropores in mesoporous materials is yet another useful tool for porous system engineering.

2. Experimental

Three samples were used in the present study. The first, C8 MCM-41 was prepared in the presence of OTAB as reported earlier [15]. A mixture of 5 g of Cab-O-Sil M5 silica and 32.2 g of water was stirred vigorously for 10 min, before adding a solution of 11.2 g of OTAB in 108.8 g of water. After an additional 10 min of stirring, a solution consisting of 14.36 g of tetramethylammonium silicate (10 wt% SiO_2) and 6.82 g of sodium silicate (28 wt% SiO_2, 10 wt% Na_2O) was added. The mixture was aged for 30 min under stirring, then transferred into a Teflon-lined autoclave and heated under autogenous pressure at 373 K for 24 h with no stirring. The other two samples, C8TR413 and C8TR423 MCM-41 were prepared at 343 K and thermally restructured at 413 and 423 K, respectively. The synthesis was carried out as reported elsewhere [19,20] using the following gel composition $1SiO_2$:0.33TMAOH:0.17OTAB:0.17NH_4OH :17H_2O. Cab-O-Sil M-5 silica (3.6 g) was mixed manually with 6 g of water and then 6.16 g of 25 wt% tetramethylammonium hydroxide (TMAOH) was added. 2.53 g of OTAB was dissolved in 6.56 g of water and subsequently 1.17 g of 30 wt% NH_4OH was introduced. The mixture containing silica and OTAB was stirred for ca. 30 min, then transferred into a Teflon-lined autoclave and treated under autogenous pressure without stirring, at 343 K for 3 days. The autoclave was transferred to another oven preheated at the desired temperature (413 or 423 K) and kept for 48 h.

All samples were filtered, washed with deionized water, and dried in static air at 373 K. The calcination was carried out in two steps. The material was first heated under flowing dry nitrogen to 813 K at a rate of 1 K min^{-1}. After 1 h at 813 K, nitrogen was slowly switched to dry air and the sample was heated at the same temperature for an additional period of 4 h.

Samples were characterized by X-ray powder diffraction (XRD) using a Siemens D5000 diffractometer with a nickel filtered Cu Kα radiation. Nitrogen adsorption–desorption measurements were performed as reported earlier [15,19,23,24] using a volumetric adsorption analyzer ASAP 2010 from Micromeritics, Norcross, GA. The samples under study were degassed for 2 h at 473 K and subsequently the measurements were carried out at 77 K over a wide relative pressure range from ca. 10^{-6} to 0.995.

3. Methodology

Adsorption data were used to obtain information about surface and structural properties of the samples under study. It should be noted that according to IUPAC recommendations [25], pores are classified as micropores (width $w < 2$ nm), mesopores (2 nm $< w <$ 50 nm) and macropores ($w > 50$ nm). Moreover, in the current work, pores that belong to the ordered mesoporous structure of MCM-41 materials will be referred to as primary mesopores, whereas other mesopores present in the samples will be designated as secondary mesopores. The specific surface area was assessed using the BET method [25,26] from adsorption data in a relative pressure range from 0.04 to 0.1. The external surface area S_{ex} (i.e., that of macropores and secondary mesopores), the total surface area S_t (which excludes the surface area of micropores present in the samples), primary mesopore volume V_p and micropore volume V_{mi} were obtained from the high resolution α_s-plot method [19,26]. LiChrospher Si-1000 (EM Separations, Gibbstown, NJ) served as the macroporous reference adsorbent. The total surface area S_t was calculated using the formula $S_t = (\eta_l S_{BET,ref})/\nu_{0.4,ref}$, where $S_{BET,ref}$ and $\nu_{0.4,ref}$ are the BET specific surface area and the amount adsorbed at $p/p_0 = 0.4$ for the reference adsorbent; η_l is the slope of the α_s-plot at low pressure between the relative pressure for which micropores, if present, are completely filled and the relative pressure corresponding to the beginning of nitrogen condensation in primary mesopores. The primary mesopore surface area S_p was calculated as the difference between the total surface area S_t and the external surface area S_{ex}. The total pore volume V_t was assessed from the adsorbed amount at a relative pressure of 0.99 by converting it to the corresponding volume of liquid adsorbate.

The pore size of the C8 MCM-41 sample was assessed from the XRD (100) interplanar spacing d and the primary mesopore volume V_p on the basis of geometrical considerations of a uniform hexagonally packed array of infinite cylindrical pores [15]. Under the latter assumptions, the pore diameter w_d can be obtained as:

$$w_d = cd\left(\frac{\rho V_p}{1+\rho V_p}\right)^{1/2}, \quad (1)$$

where ρ is the density of pore walls, assumed to be equal to 2.2 g/cm^3 [15] and $c = [8/(3^{1/2}\pi)]^{1/2} = 1.213$ is a constant. In eq. (1), the term in brackets represents the ratio of the specific (i.e., per 1 g of MCM-41 material) primary mesopore volume V_p to the sum of the latter and the volume occupied by the pore walls (equal to $1/\rho$). The pore wall thickness was assessed as the difference between the unit cell parameter $a = 2/3^{1/2}\, d$ (i.e., distance between the centers of adjacent pores) and the pore size w_d. A modified version of eq. (1) was used for the thermally restructured samples (C8TR413 and C8TR423) to account for the presence of micropores, which were assumed to be holes in the primary mesopore walls:

$$w_d = cd\left(\frac{V_p}{1/\rho + V_p + V_{mi}}\right)^{1/2}. \quad (2)$$

In eq. (2), the term in brackets corresponds to the ratio of the specific volume of primary mesopores V_p to the sum of the specific volumes of the pore walls ($1/\rho$), the micropores (V_{mi}) and the primary mesopores (V_p).

The pore size distributions in the mesopore range were calculated from adsorption branches of the isotherms using the Barrett–Joyner–Halenda (BJH) method [16] with the modified Kelvin equation suitable for accurate assessment of pore sizes, especially for MCM-41 materials [24]. The modified Kelvin equation assumes the form [24]:

$$r(p/p_0) = \frac{2\gamma V_L}{RT\ln[(p/p_0)]} + t(p/p_0) + 0.3\ \text{nm}. \quad (3)$$

The statistical film thickness curve $t(p/p_0)$ was based on an adsorption isotherm for LiChrospher Si-4000 macroporous silica gel (which was acquired in the relative pressure range from ca. 10^{-5} to 0.985), but can be accurately represented for p/p_0 from 0.1 to 0.95 [24] by the Harkins–Jura equation:

$$t(p/p_0) = 0.1\left[\frac{60.65}{0.03071 - \log(p/p_0)}\right]^{0.3968}, \quad (4)$$

where t is expressed in nanometers. In eqs. (3) and (4), p and p_0 are the equilibrium vapor pressure and saturation vapor pressure of nitrogen adsorbate, $\gamma = 8.88 \times 10^{-3}$ N/m is its surface tension at temperature $T = 77$ K, $V_L = 34.68$ cm^3/mol is its molar volume and $R = 8.314$ J mol^{-1} K^{-1} is the universal gas constant.

For comparative purposes, the pore size distributions for the samples under study were also calculated using the DFT program [27]. Further details on the characterization of mesoporous molecular sieves by means of nitrogen adsorption and the calculation methods used can be found elsewhere [15,19,23,24].

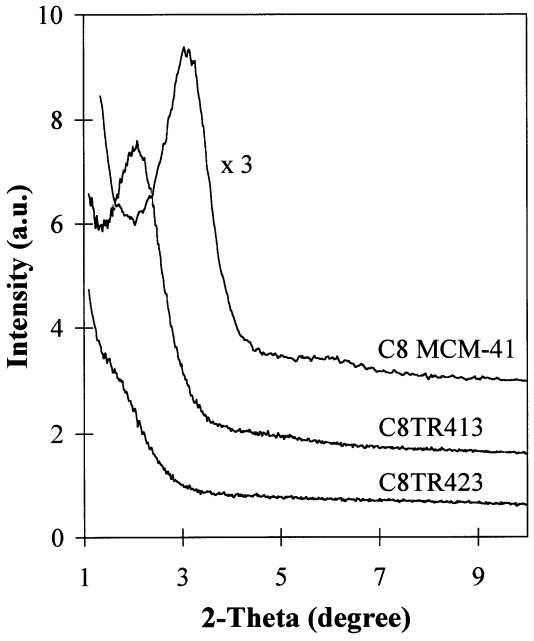

Figure 1. X-ray diffraction patterns for MCM-41 samples.

4. Results and discussion

Figure 1 shows the XRD patterns for the three samples under study. The corresponding d distances are listed in table 1. As seen, our samples exhibit only one rather broad XRD peak. Nonetheless, as demonstrated below, they have interesting pore structures and other textural properties.

Nitrogen adsorption isotherms for our MCM-41 samples are shown in figures 2 and 3, and their textural properties are listed in tables 1 and 2. As reported previously [15], adsorption on C8 MCM-41, which was synthesized in a conventional manner, increases markedly with the relative pressure up to about 0.15 and then levels off, indicating that the condensation in primary mesopores is essentially completed. A subsequent increase in the adsorbed amount can be attributed to the multilayer adsorption on the external surface area of the sample, followed by the capillary condensation in secondary mesopores at a relative pressure above ca. 0.9.

Table 1
Structural properties of MCM-41 materials [a]

Sample	d (nm)	a (nm)	w_d (nm)	b_d (nm)	w_{BJH} (nm)	w_{DFT} (nm)
C8 MCM-41	2.8	3.3	2.1	1.2	2.3	2.0
C8TR413	4.2	4.8	3.1	1.7	2.8	2.5
C8TR423	5.4	6.3	3.0	3.3	2.8	2.5

[a] d: (100) interplanar spacing obtained from XRD; a: unit cell parameter ($a = 2/3^{1/2}\, d$); w_d and b_d: pore diameter and pore wall thickness calculated on the basis of geometrical considerations (eqs. (1) and (2), $b_d = a - w_d$); w_{BJH} and w_{DFT}: maxima of pore size distributions calculated using the BJH method with the corrected Kelvin equation [24] and the DFT program [27], respectively.

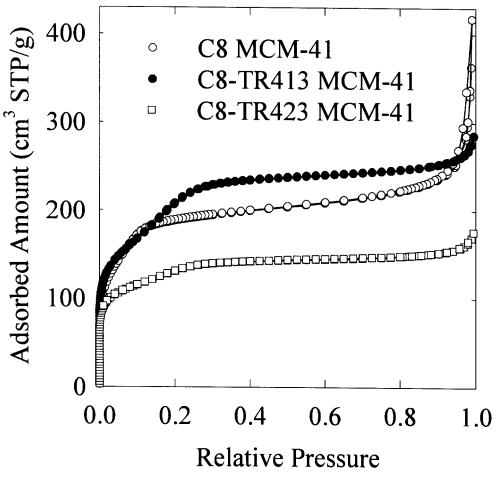

Figure 2. Nitrogen adsorption isotherms for MCM-41 samples.

For the hydrothermally restructured samples, the isotherms level off at relative pressures close to 0.3, which indicates that their primary mesopores are larger in comparison with those of C8 MCM-41. Moreover, beyond this relative pressure, further increase in the adsorbed amount is rather small, even for pressures close to the saturation pressure. This provides evidence of low external surface areas and secondary mesopore volumes of the C8TR413 and C8TR423 materials.

Adsorption isotherms shown in the logarithmic scale (figure 3) reveal that the course of low-pressure adsorption is significantly different for the sample synthesized in a conventional manner and the hydrothermally treated ones. For the former, the adsorbed amount increases gradually with the relative pressure, as is the case for mesoporous silica gels [28] and many MCM-41 materials [15,29,30]. However, the amount adsorbed on the hydrothermally restructured samples was significantly

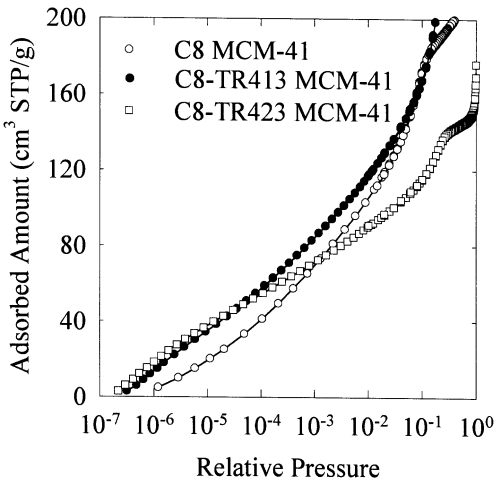

Figure 3. Low-pressure parts of nitrogen adsorption isotherms for MCM-41 samples.

Table 2
Pore volume and surface area of the MCM-41 samples [a]

Sample	S_{BET} (m^2g)	V_t (cm^3/g)	V_{mi} (cm^3/g)	S_p (m^2/g)	V_p (cm^3/g)	S_{ex} (m^2/g)
C8 MCM-41	760	0.65	(0.01)	510	0.25 (0.24)	120
C8TR413	700	0.43	0.04	530	0.30	50
C8TR423	460	0.26	0.07	260	0.13	30

[a] S_{BET}: BET specific surface area; V_t: total pore volume; V_{mi}: micropore volume; S_p: surface area of primary mesopores; V_p: primary mesopore volume, S_{ex}: external surface area.

larger, particularly at the lowest end of relative pressures (below 10^{-4}). All three samples under study are siliceous in nature, so their surface properties with respect to nitrogen are expected to be very similar, since it was shown that the latter properties are not influenced in any noticeable extent by details of the mesoporous structure of the materials [15,19,23,28,29]. Therefore, the low-pressure adsorption behavior of the hydrothermally restructured materials is most likely associated with the occurrence of significant microporosity [19,31]. Such a microporous character of the hydrothermally treated samples is in agreement with our previous study [19] of post-synthesis restructuring of C16 MCM-41 materials synthesized in the presence of CTAB. It was shown that excessive hydrothermal treatment leads to the development of microporosity, presumably as a result of the degradation of the mesopore wall structure. The latter was found to be increasingly inhomogeneous with broken walls and missing parts [20], so one can expect that the micropores present in the currently studied samples are holes in the pore walls. Additional support for this contention will be provided later.

The BET specific surface areas for the samples are listed in table 2. Due to the presence of microporosity, these data may be somewhat inaccurate, but it is clear that C8TR423 has a much smaller surface area than the two other samples. Application of the high resolution α_s-plot method [19,26,29,32] allowed for an assessment of the micropore and primary mesopore volumes and provided more reliable information about surface area of the samples (table 2). Primary mesopore surface areas S_p of the C8 MCM-41 and C8TR413 samples occurred to be close to each other (about 500 m^2/g) and twice as large as S_p for C8TR423. The primary mesopore volumes for all three materials were rather low in comparison to MCM-41 samples with larger pore sizes [2,15,19,29]. It is also worth mentioning that the external surface areas and secondary mesopore volumes ($V_t - V_p - V_{mi}$) of the hydrothermally treated MCM-41 materials were relatively low, which is in agreement with previous studies on MCM-41 samples of larger pores, restructured under similar conditions [19].

The low pressure parts of the α_s-plots for the materials under study are shown in figure 4. It can be noticed that the initial part of the plot for C8 MCM-41 exhibits

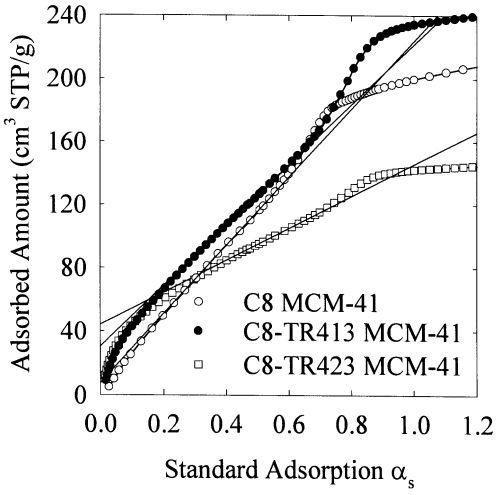

Figure 4. High-resolution α_s-plots for the MCM-41 samples. Adsorbed amounts corresponding to intercepts of the lines drawn through the linear parts of the plots are proportional to the micropore volume of the samples.

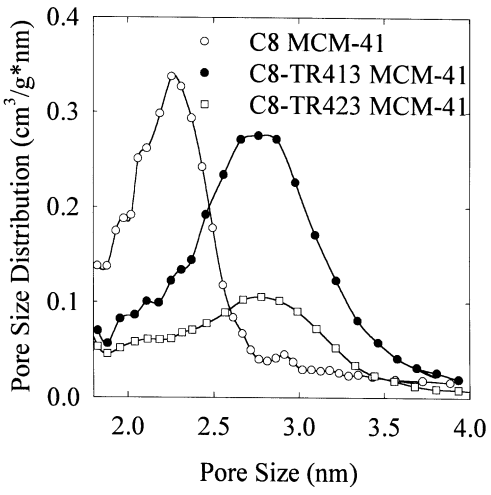

Figure 5. Primary mesopore size distributions for the MCM-41 samples calculated using the Barrett–Joyner–Halenda method with the corrected Kelvin equation.

quite good linearity, although a slight downward deviation takes place for α_s below ca. 0.15 (relative pressure below 10^{-4}). The latter behavior is indicative of microporosity, but it can also arise from enhanced interactions of nitrogen molecules with the pore surface of considerable curvature, as discussed elsewhere [15,24]. Therefore, in table 2, the micropore volume V_{mi} and the primary mesopore volume V_p (corrected for the possible presence of microporosity) for the C8 MCM-41 are written in brackets. In the case of the hydrothermally restructured samples, the initial parts of the α_s-plots are markedly bent downwards, providing a clear evidence of microporosity. For both samples, the nonlinear part of the plot was followed first by a linear segment in the α_s range from ca. 0.3 to 0.6, then by a pronounced upward swing due to the condensation of nitrogen in primary mesopores. The presence of the linear segment indicates that after a relative pressure of ca. 0.001 (which corresponds to α_s equal to 0.3) is reached, the adsorption proceeds in a similar way as for the nonporous reference adsorbent until the onset of the condensation in primary mesopores. These observations allow us to draw two conclusions. Firstly, this suggests that the micropores are essentially filled at low relative pressures (about 0.001) and therefore are expected to be rather narrow, probably below 1 nm in width. Secondly, since the filling of micropores takes place for pressures much lower than those corresponding to the beginning of the condensation in primary mesopores, it is inferred that the pore size distributions for the C8TR413 and C8TR423 samples are bimodal with both micropores and significantly larger primary mesopores.

The BJH method [16] with the corrected Kelvin equation [24] was used to calculate the mesopore size distributions for the MCM-41 samples under study (figure 5). It can be seen that the primary mesopores of the C8 MCM-41 sample are narrower than those of the hydrothermally restructured samples and their size is at the borderline between the micropore and the mesopore range, i.e., close to 2 nm. The assumptions of the method are not valid for smaller pores, i.e., in the micropore size range [33], and therefore the BJH procedure cannot be used to analyze the microporosity of the samples.

The hydrothermally treated MCM-41 materials show quite poor XRD spectra (figure 1) with just one broad small angle peak. Despite this, an attempt was made to compare the primary mesopore diameter values obtained from the modified BJH method [23] with pore diameter values calculated on the basis of eq. (2), which assumes the hexagonal arrangement of primary mesopores and takes into account the presence of micropores (holes) in the pore walls. Interestingly, eq. (2) allowed to qualitatively reproduce the results of the modified BJH method (table 1). This agreement strongly indicates that although the mesoporous structures of the thermally restructured C8 samples are quite nonuniform, as indicated by their XRD spectra, they still possess a hexagonal arrangement of pores characteristic of MCM-41. It also needs to be noted that the calculated pore wall thicknesses for the C8TR413 and C8TR423 samples are larger than those obtained for MCM-41 samples using the same method (eq. (1)), typically in the range from 0.65 to 1.1 nm [15,19,29]. The pore wall thickness for the C8TR423 seems to be exceptionally large (3.3 nm). It should however be mentioned that a considerable amount of micropores is likely to be present in the walls of this material.

Finally, some comments need to be made about the application of the recently developed DFT method [27], which allows to obtain pore size distributions in both the micropore and the mesopore size ranges. This advanced

method was developed for carbonaceous materials of slit-like pore geometry. Since the surface properties of porous carbons and silicas are markedly different [28,31] and the pore geometry of MCM-41 is rather cylindrical, application of the current version of DFT method [27] to MCM-41 silicates may not be straightforward. Indeed, the DFT method indicates a considerable amount of micropores even for MCM-41 samples, which are completely nonmicroporous. As seen in figure 6, the pore size distribution from the DFT method for C8 MCM-41 suggests a significant microporosity (ca. 0.12 cm^3/g of micropores below 1.5 nm in diameter), whereas the comparative plot analysis shows a very small amount of micropores, if any. Therefore, the current version of the DFT method [27] is not appropriate for the assessment of the microporosity of MCM-41 materials. However, it can be used to estimate the size of primary mesopores, since the agreement with the results of the corrected BJH method and the pore size from the geometrical considerations (eqs. (1) and (2)) is quite satisfactory (table 2). It also should be noted that the Horváth–Kawazoe (HK) method [14] commonly used for micropore analysis was recently shown to indicate the presence of micropores even for macroporous carbon samples [34]. Thus, the HK method may suffer similar drawback when applied to porous silicas as we often observe on MCM-41 silicates [35]. Indeed, the only report on MCM-41 silicates which presumably contain significant amounts of micropores was based on the HK method [36]. This may actually be an artifact since the materials were prepared under rather standard conditions. Therefore, comparative plot methods, such as α_s-plot, seem to be the only reliable technique currently available to detect and quantify microporosity of MCM-41 samples. It should be kept in mind that suitable reference adsorption data are required for accurate comparative plot analysis.

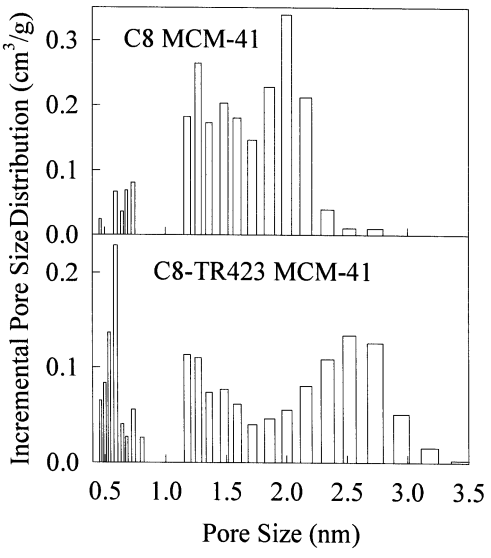

Figure 6. Pore size distributions calculated using the DFT program.

In conclusion, thermal restructuring of MCM-41 samples prepared in the presence of OTAB afforded materials with bimodal pore size distribution comprised of mesopores with an average size of ca. 3 nm and micropores below ca. 1 nm in diameter. This technique is yet another tool for engineering pore sizes and distributions to be added to the number of already well documented techniques such as vapor phase deposition, dealumination, and the use of different templates and expander molecules.

References

[1] C.T. Kresge, M.E. Leonowicz, W.J. Roth, J.C. Vartuli and J.S. Beck, Nature 359 (1992) 710.
[2] J.S. Beck, J.C. Vartuli, W.J. Roth, M.E. Leonowicz, C.T. Kresge, K.D. Schmitt, C.T.-W. Chu, D.H. Olson, E.W. Sheppard, S.B. McCullen, J.B. Higgins and J.L. Schlenker, J. Am. Chem. Soc. 114 (1992) 10834.
[3] S. Inagaki, A. Koiwai, N. Suzuki, Y. Fukushima and K. Kuroda, Bull. Soc. Chem. Soc. Jpn. 69 (1996) 1449, and references therein.
[4] A. Sayari, Stud. Surf. Sci. Catal. 102 (1996) 1.
[5] A. Sayari and P. Liu, Microporous Mater. (1997), in press.
[6] Y. Yang, N. Coombs, I. Sokolov and G.A. Ozin, Nature 381 (1996) 589.
[7] H.P. Lin and C.Y. Mou, Science 273 (1996) 765.
[8] Q.S. Huo, J.L. Feng, F. Schüth and G.D. Stucky, Chem. Mater. 9 (1997) 14.
[9] Y. Yang, N. Coombs and G.A. Ozin, Nature 386 (1997) 692.
[10] P.T. Tanev and T.J. Pinnavaia, Science 271 (1996) 1267.
[11] P. Liu, I.L. Moudrakovski, J. Liu and A. Sayari, Chem. Mater. (1997), in press, and references therein.
[12] A. Sayari, Chem. Mater. 8 (1996) 1840.
[13] C.C. Freyhardt, M. Tsapatsis, R.F. Lobo, K.J. Balkus Jr. and M.E. Davis, Nature 381 (1996) 285.
[14] G. Horváth and K. Kawazoe, J. Chem. Eng. Jpn. 16 (1983) 470.
[15] M. Kruk, M. Jaroniec and A. Sayari, J. Phys. Chem. B 101 (1997) 583.
[16] E.P. Barrett, L.G. Joyner and P.P. Halenda, J. Am. Chem. Soc. 73 (1951) 373.
[17] P.I. Ravikovitch, S.C.O. Domhnaill, A.V. Neimark, F. Schüth and K.K. Unger, Langmuir 11 (1995) 4765.
[18] P.I. Ravikovitch, D. Wei, W.T. Chueh, G.L. Haller and A.V. Neimark, J. Phys. Chem. B 101 (1997) 3671.
[19] A. Sayari, P. Liu, M. Kruk and M. Jaroniec, Chem. Mater. 9 (1997), in press.
[20] D. Khushalani, A. Kuperman, G.A. Ozin, K. Tanaka, J. Garces, J.J. Olken and N. Coombs, Adv. Mater. 7 (1995) 842.
[21] A. Sayari, I.L. Moudrakovski, C.I. Ratcliffe, J.A. Ripmeester and K.F. Preston, J. Phys. Chem. 99 (1995) 16373.
[22] A. Keshavaraja, V. Ramaswamy, H.S. Soni, A.V. Ramaswamy and P. Ratnasamy, J. Catal. 157 (1995) 501.
[23] M. Kruk, M. Jaroniec and A. Sayari, Microporous Mater. 9 (1997) 173.
[24] M. Kruk, M. Jaroniec and A. Sayari, Langmuir (1997), in press.
[25] K.S.W. Sing, D.H. Everett, R.A.W. Haul, L. Moscou, R.A. Pierotti, J. Rouquerol and T. Siemieniewska, Pure Appl. Chem. 57 (1985) 603.
[26] S.J. Gregg and K.S.W. Sing, *Adsorption, Surface Area and Porosity* (Academic Press, London, 1982).
[27] J.P. Olivier, W.B. Conkin and M. v. Szombathely, in: *Characterization of Porous Solids III*, eds. J. Rouquerol, F. Rodrigues-Reinoso, K.S.W. Sing and K.K. Unger (Elsevier, Amsterdam, 1994) p. 81.

[28] Y. Bereznitski, M. Jaroniec, M. Kruk nad B. Buszewski, J. Liquid Chromatogr. 19 (1996) 2767.
[29] M. Kruk, M. Jaroniec, R. Ryoo and J.M. Kim, Microporous Mater. (1997), in press.
[30] M.W. Maddox, J.P. Olivier and K.E. Gubbins, Langmuir 13 (1997) 1737.
[31] M. Kruk, M. Jaroniec and Y. Bereznitski, J. Colloid Interf. Sci. 182 (1996) 282.
[32] K. Kaneko, C. Ishii, M. Ruike and H. Kuwabara, Carbon 30 (1992) 1075.
[33] C. Lastoskie, K.E. Gubbins and N. Quirke, J. Phys. Chem. 97 (1993) 4786.
[34] M. Kruk, M. Jaroniec and J. Choma, Adsorption 3 (1997) 209.
[35] A. Sayari, unpublished.
[36] C.J. Guo, Stud. Surf. Sci. Catal. 97 (1995) 165.